processes

MDPI

Article

Numerical Investigation and Optimization of the Flow Characteristics of Bend Pipe with Different Bending Angles

Jianyi Zhang *, Dongrui Wang, Weiwei Wang and Zuchao Zhu

Key Laboratory of Fluid Transmission Technology of Zhejiang Province, Zhejiang Sci-Tech University, Hangzhou 310018, China; wangdongdongrui@163.com (D.W.); wangww0619@163.com (W.W.); zhuzuchao@zstu.edu.cn (Z.Z.)

* Correspondence: zdreamx@zstu.edu.cn

Abstract: The bend pipe with a circular section, which is widely used in hydropower, chemical industry and other fields, is a common form in pipeline systems. However, secondary flow occurs when the fluid flows through the bend pipe, thereby affecting the stability of the pipeline system. Different bending angles have various effects. Therefore, this paper establishes 3D models of a circular bend pipe with different bending angles. The influence of bending angle on flow field distribution and downstream flow is analyzed numerically. The larger the bending angle is, the more obvious the flow distribution and even the unevenness at the elbow will be, hence resulting in poor stability. The distance required to restore flow uniformity also increases. The pressure energy loss of the bend pipe with different bending angles is investigated. Results show that with the increase in bending angle, the global pressure loss presents a trend of "increase-decrease-increase." The closer the bending angle is to 90°, the greater the influence of centrifugal force is on the flow, and the more obvious the secondary flow phenomenon will be. Aiming at the nonuniformity phenomenon, the structure optimization of a 90° bend pipe with the greatest influence is conducted. The improvement of the flow characteristics of bend pipe with different thick-diameter ratio and length-diameter ratio is compared. The deflector with a certain thickness can enhance the uniformity, safety and useful life of the bend pipe. The sharp-end length can improve the velocity uniformity to a certain extent but has minimal influence on flow characteristics compared with the thick-diameter ratio. This paper aims to study and improve the flow performance of a multi-structure bend pipe to make it suitable for more complex conditions.

Keywords: bend pipe; secondary flow; numerical simulation; bending angle; structure optimization

Citation: Zhang, J.; Wang, D.; Wang, W.; Zhu, Z. Numerical Investigation and Optimization of the Flow Characteristics of Bend Pipe with Different Bending Angles. *Processes* **2022**, *10*, 1510. https://doi.org/10.3390/pr10081510

Academic Editor: Haiping Zhu

Received: 5 July 2022
Accepted: 24 July 2022
Published: 1 August 2022

1. Introduction

The circular bend pipe is a common form in a pipeline system, and plays a role in changing the fluid direction. It is widely used in various fields such as water conservancy and hydropower [1], the energy and chemical industries [2–5], and in biomedicine [6]. However, when the fluid flows through the elbow, the flow inertia force becomes much greater than the wall viscous force, thereby causing the fluid to separate on the intrados of the elbow and impact the extrados. The inertia in the bend pipe is expressed as centrifugal force, hence causing the flow to deviate parallel to the pipe wall and results in a secondary flow. Dean vortex [7] is a typical form of secondary flow in the bend pipe system. It enhances the nonuniformity [8] and instability [9] of the pipeline system, and it can also improve the mass and heat transfer performance of the fluid [10]. Therefore, it is of great significance to study the flow in a bend pipe.

At present, the research on flow in a bend pipe is mainly focused on different flow characteristics under fixed bending angles. Among them, the most widely used one, the 90° bend pipe, is the main object of this research. The experiment can reflect the realest flow law in the bend pipe. Kalpakli et al. studied the turbulent flow field and vortex

characteristics downstream of a 90° bend pipe by stereoscopic particle image velocimetry. The vortex switching phenomenon of a Dean vortex in unsteady flow [11] and oscillation behavior in steady flow [12] were revealed. The stability caused by oscillation is a hot topic in the research of the bend pipe. With the help of direct numerical simulation, the flow stability of 90° bend pipe under Re = 2000–3000, curvature of 0.33 [13] and Re = 5000, curvature of 0.4 [14] were studied. The finding shows that the bending of the pipe enhanced instability and reached an extreme 1*D* downstream of the bend pipe, whereas the initial instability occurred at 15° of the elbow inlets. Wang et al. [15] conducted a numerical simulation research on three typical combinations of 90° bend pipe from the pressure loss and streamline, and obtained the arrangement form of a bend pipe with the best flow stability. Under the condition of constant curvature, the curvature ratio of the elbow is an important factor that affects the flow characteristics of pipes. The bend pipe with low curvature ratio has obvious flow separation [16]. The bend pipe with high curvature ratio has a more uniform flow field distribution [17]. Zhang et al. [18] derived the formula for calculating the pressure of Newtonian fluid in a 90° bend pipe with different curvature ratios. Chowdhury et al. [19] found that different curvature ratios would cause differences in pressure distribution and loss coefficient of the bend pipe. The flow characteristics in the 90° bend pipe have a great influence on the stability and safety of the pipeline.

Other bend pipes are often used in daily life and engineering applications [20]. Compared with a 90° bend pipe, various bending leads to different fluid flow directions [21], which affect the centrifugal force generated when passing through the elbow, thereby resulting in different physical laws such as flow and heat transfer [22]. Therefore, it has important research value for different bending. Zhang et al. [23] analyzed the transient characteristics of a bend pipe with different bending in the leakage process, and found that the periodic attenuation of downstream flowrate and pressure curves of a bend pipe was not significantly affected by the bending coefficient (i.e., the ratio of the curvature radius of the elbow to the pipe diameter). In addition, through the finite element method, scholars studied the influence of bending on pipeline safety under different pressure conditions [24–26] and proposed the plastic load solution of bend pipes [27]. The present research on different bending is mainly focused on the load and deformation of the solid part, whereas the internal flow law is unclear. Differences are observed between the secondary flow and Dean vortex at different elbows, and their influence on flow characteristics cannot be ignored. They not only exert force on the pipe wall but also affect the development of downstream flow. Therefore, its mechanism should be studied to provide a more perfect theoretical basis.

In view of the stability and safety problems found in the studies, the researchers also began to optimize and adjust the structure of the bend pipe to obtain the ideal flow field distribution and better external characteristics [28]. Two main structural optimization methods can be applied for the bend pipe: wall modification [29] and deflector installation [30], both of which were aimed at elbow. The wall modification of the elbow could reduce pressure drop and vortex magnitude. However, it did not fundamentally solve the flow problem caused by secondary flow. The deflector installed at the elbow could effectively inhibit the influence of secondary flow and improve the flow uniformity in the pipe, which had considerable application value. However, the present research on this is simple and imperfect.

In conclusion, the flow characteristics of bend pipe with different bending angles must be studied and optimized. Therefore, in this paper, 3D circular bend pipe models with different bending angles are established. The flow inside the bend pipe is simulated by the commercial software Fluent©. The effect of bending angle on the flow characteristics of bend pipes is analyzed, and the numerical results are verified by existing literature. By means of pressure and drag coefficients, the global pressure loss and downstream pressure distribution of the elbow are discussed. The flow direction and radial development of downstream velocity at different bending angles are compared. On this basis, the local optimization of the elbow structure is conducted by adding three deflectors which reduce

flow nonuniformity and instability. The effects of different sharp-end thickness and length on flow field and related performance are compared to obtain improved flow characteristics. This paper aims to study and improve the flow characteristics of a multi-structure bend pipe to make it suitable for more complex conditions.

2. Physical and Numerical Methods

2.1. Physical Models

The schematic of the physical model of the 90° bend pipe is shown in Figure 1. The cross-section of the bend pipe is designed as the most commonly used circle [31–33]. The diameter of the pipe D is 60 mm, and the curvature ratio of the elbow of the bend pipe $\gamma = D/R_B = 0.63$ (where R_B (mm) is the curvature radius of the elbow) [11]. To present the flow at the elbow from being affected by upstream and downstream flow fields and fully develop the downstream flow field to ensure the accuracy of calculation, this paper selects a straight pipe with 5D at the inlet of the elbow as the upstream calculation domain, and that with 10D at the outlet as the downstream calculation domain. The bending angle models of 5°, 30°, 60°, 120° and 180° with the same diameter and curvature ratio are also established to cover a wide range of bending angles [24,25,27]. In addition, the pipe cross-section with the distance from the elbow outlet y (mm) is extracted. The circular curve with a radius of 0.25D on the section is defined as Line A, the horizontal center line is defined as Line B, the vertical center line is defined as Line C, and the downstream center line of the bend pipe is defined as Line D.

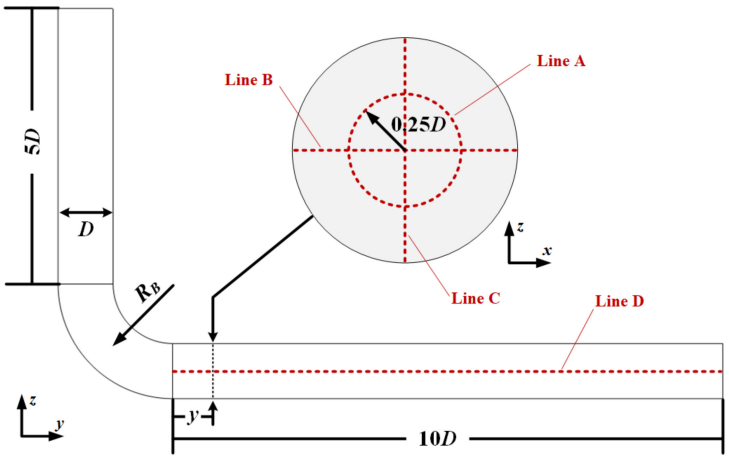

Figure 1. Schematic of the physical model (90° bend pipe for instance).

The established 3D model is meshed by ICEM software. Owing to the smooth wall surface and simple structure of the bend pipe model, hexahedral mesh with the advantages of easy solution and fast convergence is used to generate it [34]. Boundary layer refinement is carried out on the near wall of the pipeline to simulate the flow near the boundary layer accurately [35]. At the same time, given that the flow at the elbow is more complex than that at the straight pipe, the mesh at the elbow is also locally refined, resulting in the mesh shown in Figure 2. For all the investigated bend pipes, the calculation accuracy should be ensured while the calculation efficiency should be improved. Therefore, the mesh independence is verified, and the results are characterized by the pressure coefficient at the inlet and outlet (Table 1). When the number of meshes is greater than 1.7 million, the pressure coefficient of the bend pipe basically does not change with the number of meshes, that is, the number of meshes is controlled at about 1.7 million.

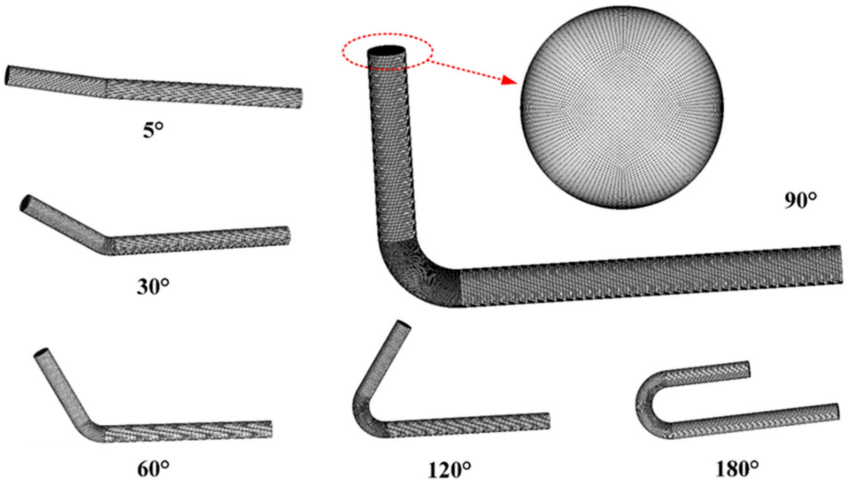

Figure 2. Mesh of the bend pipe with different bending angles.

Table 1. Mesh independence verification.

No.	Mesh Number ($\times 10^4$)	Pressure Coefficient	Relative Error (%)
1	45	1.3972	0.59
2	90	1.4055	1.03
3	140	1.4201	0.53
4	170	1.4277	0.16
5	200	1.4300	0.26
6	260	1.4336	——

2.2. Numerical Methods

Based on the ANSYS Fluent© software (Washington County, PA, USA), in this paper, the Reynolds-averaged Navier-Stokes (RANS) method [36] is used to solve the flow characteristics of a bend pipe, in which the governing equations include continuity and momentum equations [37]. For turbulence calculation, a realizable $k-\varepsilon$ model [38] with better effects on complex flows such as vortex and rotation is selected. This paper only describes the framework of the numerical models, and further details can be found in the previous study [39–42].

The flow medium at normal temperature with a Mach number below 0.3 is air, thereby exhibiting incompressibility. The inlet boundary condition is velocity-inlet, and the velocity is set as 3.41 m/s (i.e., the Reynolds number is 14,000). The outlet boundary condition is pressure-outlet, and the pressure (relative pressure) is set as 0 Pa. A no slip boundary condition is selected for the wall of the straight pipe and elbow. The SIMPLEC algorithm is used to solve the problem, and twice skewness correction is set. The momentum equation, turbulent kinetic energy, and turbulent dissipation rate are discretized using the second-order upwind scheme. In addition, the residuals of the continuity term, velocity, turbulent kinetic energy and diffusion term are all set to 10^{-5}.

Many scholars have studied the internal flow characteristics of the bend pipe. This paper verified the numerical results with the help of Kalpakli [11] and Carisson [34] to ensure the feasibility of numerical simulation methods. Under the same conditions described in the literature, numerical simulation is carried out by using the method presented in this paper. A section of $0.67D$ downstream of the elbow outlet is taken. The simulation results of velocity distribution and the streamline of this section are compared with the results of PIV [11], as shown in Figure 3a. In terms of flow field distribution, the simulation results are consistent with the experimental results [34]. In addition, the horizontal center line velocity on this section is extracted and compared with the literature results (Figure 3b).

The simulation results are basically consistent with the literature results, and the error is within the allowable range. This finding shows that the numerical method presented in this paper has certain reliability.

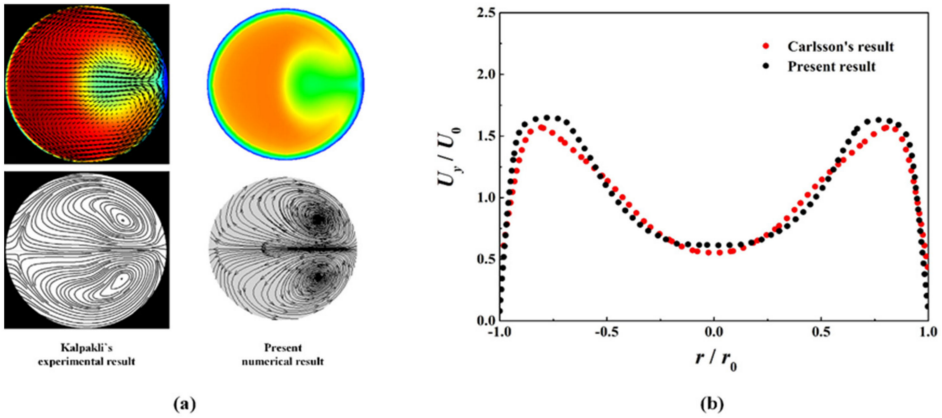

Figure 3. Verification of numerical method: (**a**) flow field distribution; (**b**) the relative velocity of the horizontal center line.

3. Results and Discussion

When the bending is different, the flow separation degree on the intrados and the impact angle with the extrados wall are diverse, resulting in the difference in pressure accumulation at the elbow. This difference leads to various degrees of secondary flow, causing different nonuniformity and even instability problems. The present research mainly focused on the deformation and load of the solid wall [23–27], but the investigation of flow characteristics with different bending angles is helpful for mastering the basic physical laws and provides a theoretical basis for structural optimization.

3.1. Global Flow Analysis

By studying the distribution of pressure and velocity, the changing law of the global flow pattern in the bend pipe with the bending angle can be obtained. The pressure distribution of the bend pipe with different bending angles is shown in Figure 4. The pressure distribution of each bending angle is similar. A local low-pressure region on the intrados of the bend pipe and a local high-pressure region on the extrados of the bend pipe are observed. This region appears when the bending angle is small. Local low-pressure regions and local high-pressure regions are exactly located at the elbow of the bend pipe. Meanwhile, with the increase in bending angle, the distribution area of the local low-pressure region and local high-pressure region also increases. This phenomenon is caused by the centrifugal force exerted on the fluid as it passes through the elbow. The pressure difference between the intrados and the extrados causes a radial pressure gradient at the elbow, thereby leading to the uneven distribution of the force, which may induce instability in the bend pipe.

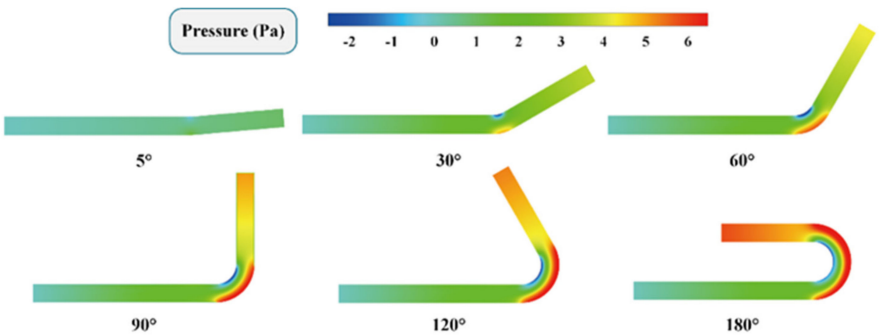

Figure 4. Pressure distribution of bend pipe with different bending angles.

The velocity distribution of the bend pipe with different bending angles is shown in Figure 5. When the fluid passes through the bend pipe, the wall constraint causes the flow direction to change. According to Bernoulli's principle, the higher the static pressure, the lower the velocity, thereby leading to low velocity in region with high pressure, whereas low pressure does the opposite. Concretely, given that the bending angle is small, the velocity is slightly affected by the bend pipe, and its velocity distribution is similar to that in the straight pipe. When the bending angle increases to 30°, the local high-velocity region begins to appear at the intrados of the elbow, whereas the local low-velocity region appears at the extrados of the elbow. An obvious low-velocity region exists in the downstream of the bend pipe near the intrados side of the elbow. With the increase in the bending angle, the area of the regions also increases.

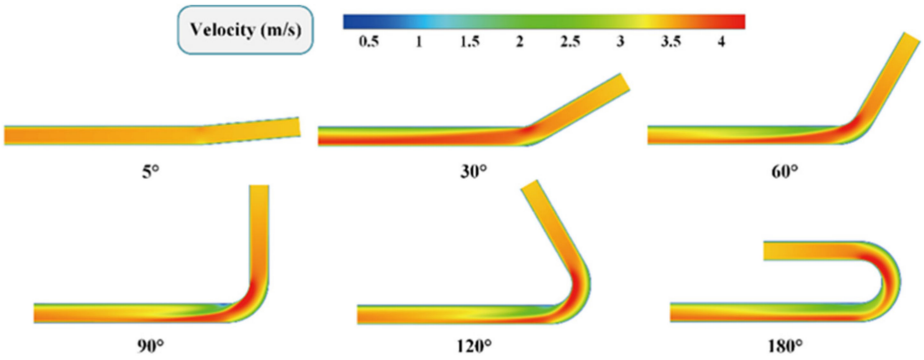

Figure 5. Velocity distribution of bend pipe with different bending angles.

3.2. Wake Development

To further study the downstream nonuniformity degree caused by secondary flow at the elbow, the average downstream pressure and velocity with different bending angle are analyzed. The velocity distribution of the downstream cross-section is compared, and the local velocity on the horizontal and vertical centerlines on the cross-section are discussed.

Pressure coefficient is a dimensionless parameter used to describe relative pressure in the flow field, which is widely used in aerodynamic research [43,44]. According to Zou's wind tunnel experiment [45], the pressure coefficient C_p can be expressed as:

$$C_p = \frac{p - p_{in}}{0.5\rho(u_{in})^2} \quad (1)$$

where p is the pressure at any point (Pa), p_{in} is the average inlet pressure (Pa), ρ is the density of the fluid (kg/m^3), and u_{in} is the average inlet velocity (m/s).

The pressure of Line A (shown as Figure 1) on the cross-section of the downstream y = 0–5D(1D) distance of the bend pipe with different bending angles is extracted as shown in Figure 6, which is characterized by the pressure coefficient. The smoother the curve is, the more uniform the pressure distribution is; and the smaller the closed area surrounded by the curve is, the smaller the relative pressure is. When the bending angle is small, the pressure downstream of the bend pipe changes slightly with the development of the flow, and the global distribution on the cross-section is uniform. With the increase in the bending angle, the relative pressure of the flow field gradually decreases, indicating that the greater the bending angles are, the more pressure energy will be consumed at the elbow. Under the influence of centrifugal force, the pressure at the outlet of the elbow is "low at the top and high at the bottom". The nonuniformity of the pressure increases with the bending angle, and reaches the maximum value at 90°. With the development of the flow, the distribution of the downstream relative pressure on the cross-section gradually becomes uniform. The distance required to restore uniformity increases with the bending angle, which indicates that the increase in the impact angle between the flow and wall enhances the degree of flow disturbance. The maximum flow impact angle is 90°, resulting in the minimum pressure

and the maximum degree of nonuniformity at this bending angle. In addition, the viscous dissipation of the pipe causes the pressure to decrease gradually with the development of flow.

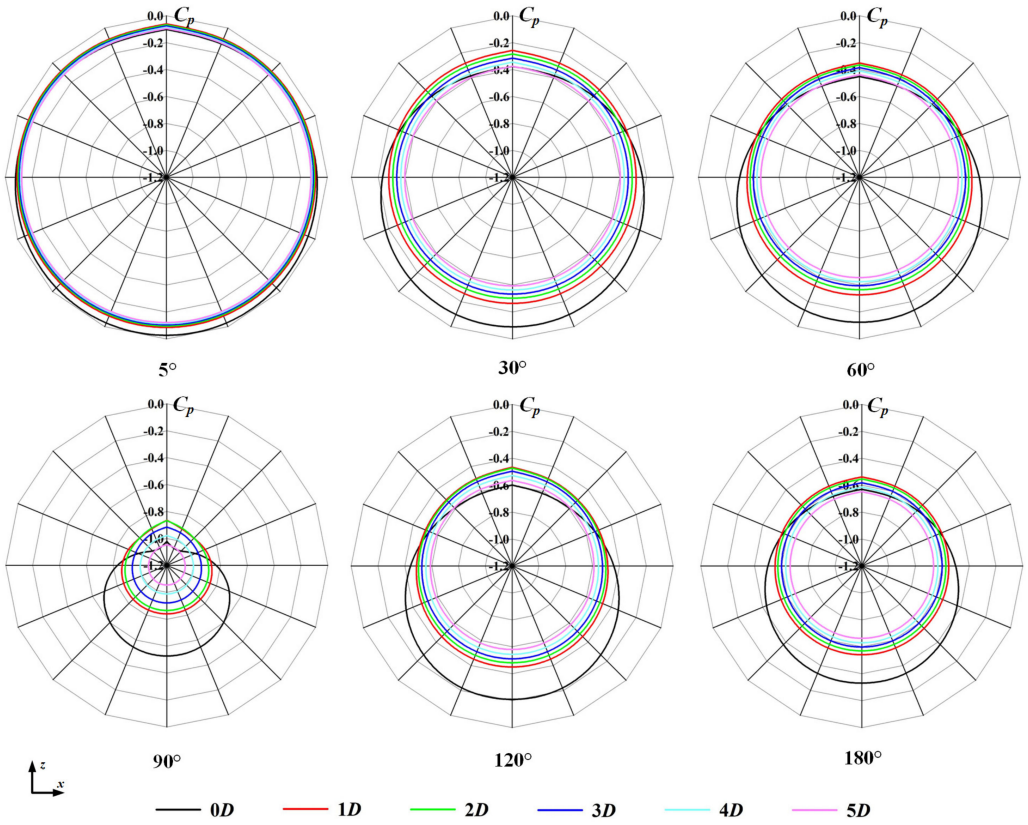

Figure 6. Pressure distribution on the downstream cross−section of the bend pipe with different bending angles.

The velocity slices of the bend pipe with different bending angles in the range of y = 0–10D downstream (shown as Figure 1) are intercepted, as shown in Figure 7. The velocity distribution at the downstream of the elbow when the bending angle is small is uniform, which is similar to that in the straight pipe. With the increase in bending angle, an obvious low-velocity region gradually appears in the cross-section. The low-velocity region at the outlet of the elbow is mainly distributed in the extrados of the elbow because the fluid impinges on the wall under the action of inertial force, so that a large amount of kinetic energy is converted into pressure energy, thereby resulting in a low velocity near the extrados. As the flow develops downstream, affected by centripetal force and pressure gradient, the flow separation occurs in the intrados of the elbow, so that the low-velocity region at the extrados gradually disappears and shifts to the intrados. The appearance of secondary flow makes air flow close to the wall, resulting in a large area of low-velocity near the center of the cross-section. The secondary flow phenomenon is most obvious when the bending angle is 90°. With the increase in the bending angle, the influence range of centripetal force and pressure gradient at the elbow increases, and the area of the intrados low-velocity region also expands. When the bending angle increases to 90°, the area of the low-velocity region changes slightly. When the flow develops to 5D downstream from the elbow outlet, the low-velocity region gradually shrinks and the flow gradually recovers uniformity. The distribution of velocity is axisymmetric.

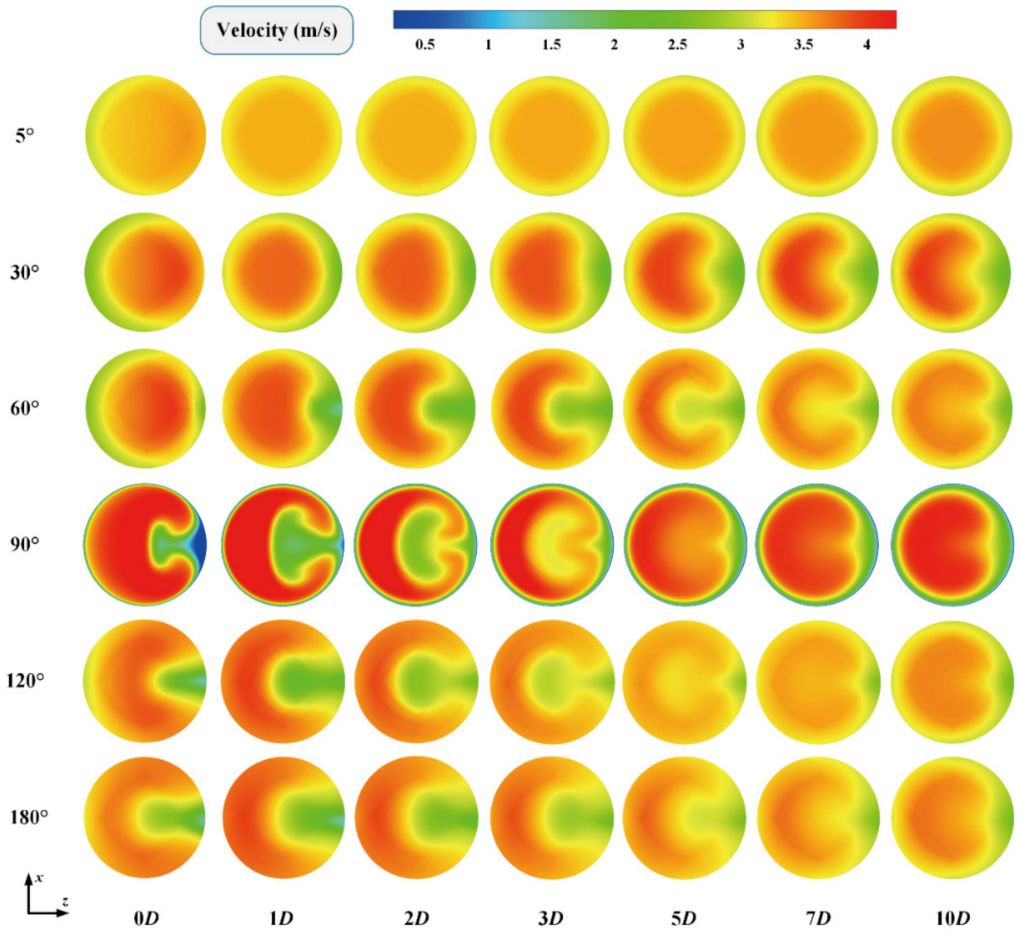

Figure 7. Velocity slices of bend pipe with different bending angles at different downstream distances.

According to the velocity slices of bend pipe at different downstream, the closer the flow is to the elbow, the more obvious the changes are with the position. To further discuss the development of downstream flow with position, the velocity of the center line 0–10*D* downstream of the elbow (Line D) with different bending angles is extracted (Figure 8). As shown in Figure 5, the inertia at the elbow causes the airflow to concentrate toward the extrados. Thus, the central velocity can be used to indicate how the flow is affected by inertia and how it develops with the flow. The velocity at the outlet of the elbow increases first and then decreases with the increase in the bending angle and reaches the maximum value at 90°. This instance indicates that the 90° bend pipe has the strongest effect on fluid acceleration. As the flow develops downstream, the center velocity of 60°, 90°, and 120° bend pipes fluctuate greatly, whereas the other bending angles fluctuate slightly. The center velocity of 90° and 120° bend pipes decreases rapidly and reaches a minimum within 2*D* of the elbow outlet, and then gradually recovers. Furthermore, the center velocity of the 60° bend pipe stays constant for the first time, then decreases after 1.5*D* from the elbow outlet, and then maintains a low velocity. This phenomenon indicates that the closer the bending angles are to 90°, the greater the influence of centrifugal force on the flow, resulting in more concentrated air flow on the extrados wall and greater nonuniformity of downstream velocity. As the flow develops downstream, the center velocity at each bending angle gradually tends to be stable, but it is still slightly larger at 90°.

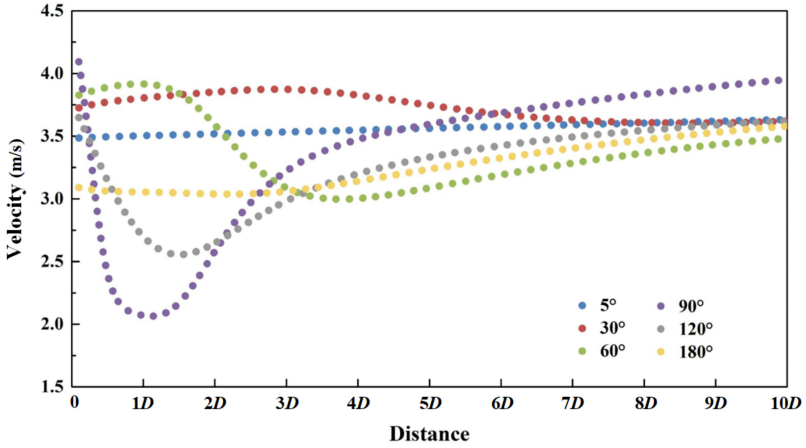

Figure 8. Velocity downstream of bend pipe with different bending angles.

The flow analysis shows that under the influence of centripetal force and pressure gradient, the obvious flow phenomenon of the bend pipe is observed near the elbow outlet, thereby forming a secondary flow. The vertical and horizontal flow characteristics at this position are investigated. The 0.67*D* cross-section downstream of the elbow outlet has been studied extensively [11,34]. Therefore, the 0.67*D* cross-section is selected as the research object in this paper. The velocity on horizontal (Line B) and vertical center lines (Line C) is extracted, and dimensionless processing is performed to obtain the velocity distributions at different bending angles (Figure 9). In the horizontal direction, the velocity is axially symmetric because it is not affected by external forces. At each bending angle, the velocity distribution is small in the center and large at both ends. With the increase in bending angle, the velocity first increases and then decreases and reaches the maximum value at 90°. When the bending angle is greater than 90°, the velocity on the horizontal center line fluctuates greatly. This phenomenon indicates that the elbow with a large bending angle is greatly affected by centripetal force and radial pressure gradient, thereby making the phenomenon of secondary flow more obvious, which corresponds to the velocity contour in Figure 7.

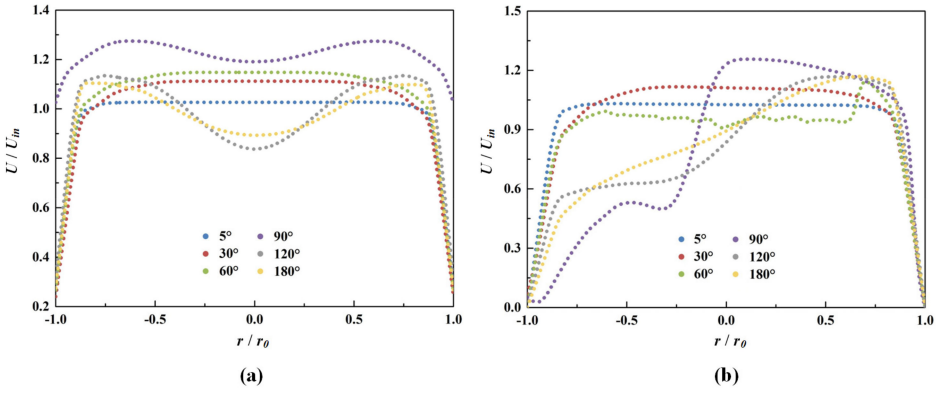

Figure 9. Velocity distribution of (**a**) horizontal and (**b**) vertical centerline at 0.67*D* cross−section of downstream bend pipe with different bending angles.

In the vertical direction, due to the centrifugal force of the elbow, as described above, the local low-velocity region occurs near the outlet of the elbow. The velocity is asymmetrical on the vertical center line, especially when the bending angle is greater than 90°. From the intrados to the extrados of the pipe, the velocity of the vertical center line of 90°, 120° and 180° bend pipe first increases and then remains unchanged (the velocity near the wall is not included here). Its velocity fluctuation is larger because the secondary flow of the 90° bend pipe is more obvious.

3.3. Pressure Loss

The formation of secondary flow in the elbow is usually accompanied by significant energy loss, and pressure energy is the most important form in the bend pipe. Therefore, the resistance coefficient is used to characterize the degree of pressure loss in this paper. Resistance coefficient is a dimensionless parameter used to describe the pressure loss caused by wall resistance in the pipeline system with relative motion, and it is an important parameter in the study of the fluid transfer system [46,47]. In the bend pipe flow [15], the resistance coefficient can be expressed as:

$$\zeta = \frac{p_{in} - p_{out}}{0.5\rho(u_{in})^2} \tag{2}$$

where p_{out} is the average outlet pressure (Pa).

The pressure loss curves of the bend pipe with different bending angles are shown in Figure 10. Almost no pressure loss is observed at small bends. With the increase in the bending angle, the pressure loss first increases, then decreases and then increases again, and reaches the maximum value when the bending angle is 90°. This shows that the secondary flow phenomenon of the 90° bend pipe is obvious, resulting in a large pressure energy loss which corresponds to the velocity fluctuation trend mentioned above. Among them, the pressure loss in the ranges of 5–30° and 60–90° has a large growth rate, while the pressure loss in the ranges of 30–60° and 120–180° has a relatively small growth rate. In the vicinity of 0° and 90°, the change in pressure loss has a more drastic fluctuation.

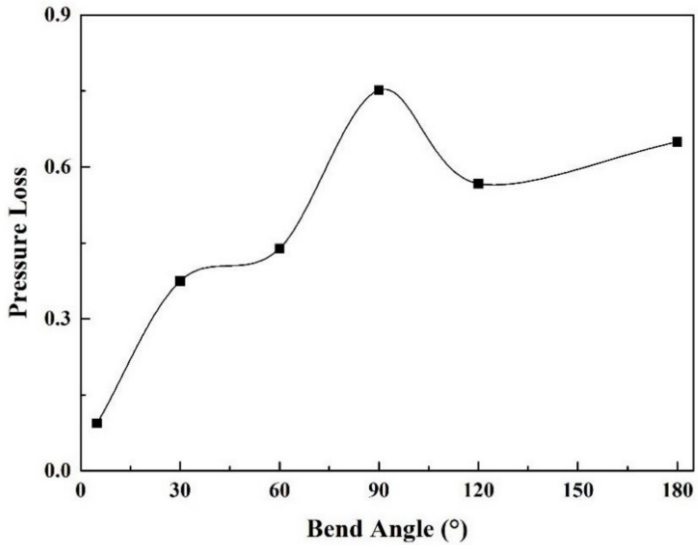

Figure 10. Pressure loss of bend pipe with different bending angles.

4. Structure Optimization

From the above analysis, it can be found that due to the influence of fluid inertia and viscosity, the flow is affected by centrifugal force when passing through the elbow, resulting in flow separation and secondary flow. Local high pressure is generated at the extrados, while low pressure is generated at the intrados, thus forming a radial pressure gradient. The secondary flow and pressure gradient leads to uneven force on the elbow and intensifies the disturbance of downstream flow, significantly affecting the safety and stability of the pipeline system.

Aiming at the phenomenon of non-uniform and unstable flow inside the bend pipe, the structure of the traditional bend pipe is optimized in this paper. The 90° bend pipe is the most widely used, and from the above analysis, it has the greatest flow fluctuation and the most severe nonuniformity. Therefore, the 90° bend pipe is selected as the research object to optimize the local structure. According to Valsala's optimization results [30], the influence

of secondary swirl can be reduced by installing flow deflectors in the elbow, and installing three flaky deflectors with sharp ends at equal spacing is better for flow straightening. That is, the curvature radius of deflector-1 is $R_{d1} = R_B - {}^1/_4 D$, that of deflector-2 is $R_{d1} = R_B$, and that of deflector-3 is $R_{d1} = R_B + {}^1/_4 D$. The deflectors extend from the elbow inlet to the outlet with a curvature parallel to the elbow wall in y-z cross-section and through the entire x-direction. Meanwhile, it has a sharp end on the upper stream side. In order to study the influence of the deflector on the flow uniformity under different geometries, two characteristic parameters (thick-diameter ratio $HD = H/D$ and length-diameter ratio $LR = L/R_B$) are defined in this paper on the basis of the Valsala optimization scheme. The improvement of flow characteristics of a bend pipe with HD = 0.02, 0.04, 0.06, 0.08, 0.10 and LR = 0.11, 0.13, 0.15, 0.20, 0.30 is compared. The schematic diagram of the optimization model is shown in Figure 11, in which R_B is the curvature radius at the center of the elbow (mm); H is the thickness of the flow deflector (mm), and all three are the same; L is the length of the sharp end of the flow deflector (mm), and all three are the same.

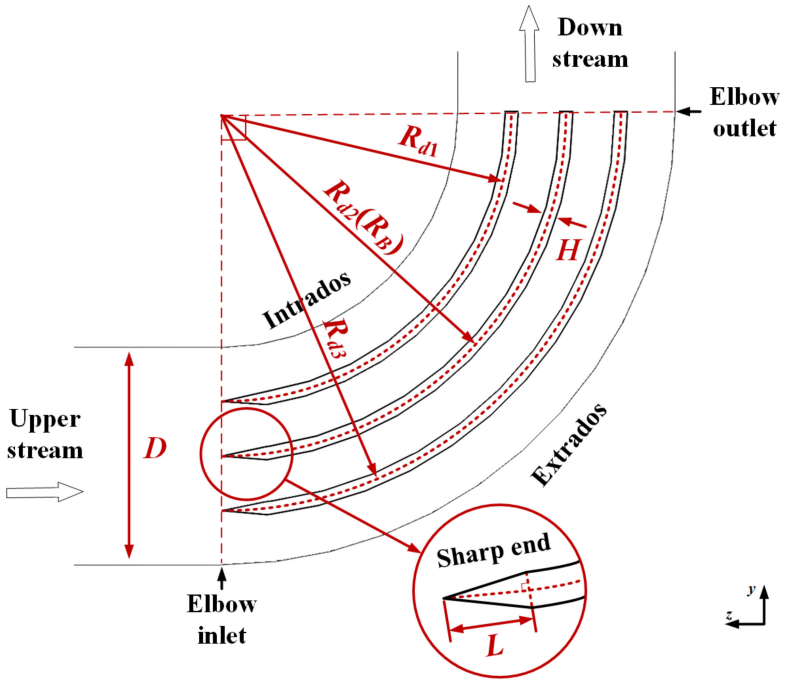

Figure 11. The schematic diagram of the optimization model.

4.1. Different Thick-Diameter Ratio

The pressure distribution in a 90° bend pipe with different thick-diameter ratio deflectors installed is shown in Figure 12, where LR is constant at 0.13 [30]. After the installation of the flow deflector, the uneven distribution of pressure in the elbow is improved effectively, but the distribution law of high extrados pressure and low intrados pressure is also retained. With the increase in HD, the area of high-pressure at the extrados of the elbow gradually decreases. The overall pressure of the elbow also shows a trend of gradual decrease and reaches an ideal state at HD = 0.06. When the HD increases to 0.08, the negative pressure region begins to appear at the elbow. The flow deflector with a certain thickness can effectively weaken the local accumulation of pressure energy at the elbow and make the pressure distribution inside the pipe more reasonable, thereby enhancing the safety and service life of the bend pipe to a certain extent.

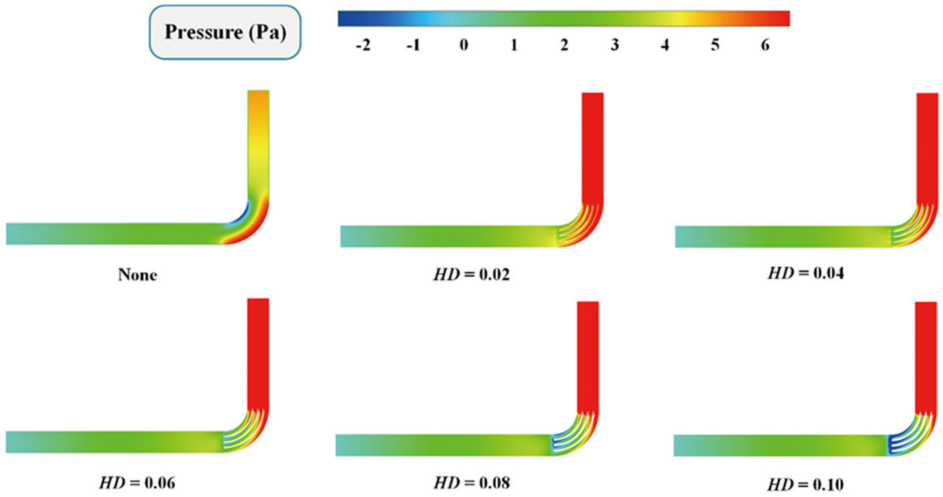

Figure 12. Pressure contour in 90° bend pipe with different thick−diameter ratio deflectors.

The 0.67*D* cross-section downstream of the elbow is cut to obtain the velocity and streamline distribution of the bend pipe with flow deflectors of different thick-diameter ratios (Figure 13). Two large Dean vortices are inside the bend pipe before optimization, which fill the whole pipe. After adding the flow deflector, the elbow part is separated into four closed regions, so the two large vortices are also decomposed into eight small vortices—each closed region appears in pairs. The velocity of the cross-section changes from a large area concentrated distribution of low-pressure region before optimization to a high- and low-pressure region spaced and evenly distributed. This shows that the effect of centrifugal force is significantly reduced. With the increase in *HD*, the velocity distribution does not change much, whereas the small vortices gradually decrease, and the energy loss caused by the secondary flow also decreases. The flow deflector with a certain thickness can reasonably adjust the structure of the secondary flow and make the velocity distribution in the pipe more uniform, thereby optimizing the flow in the bend pipe to a certain extent.

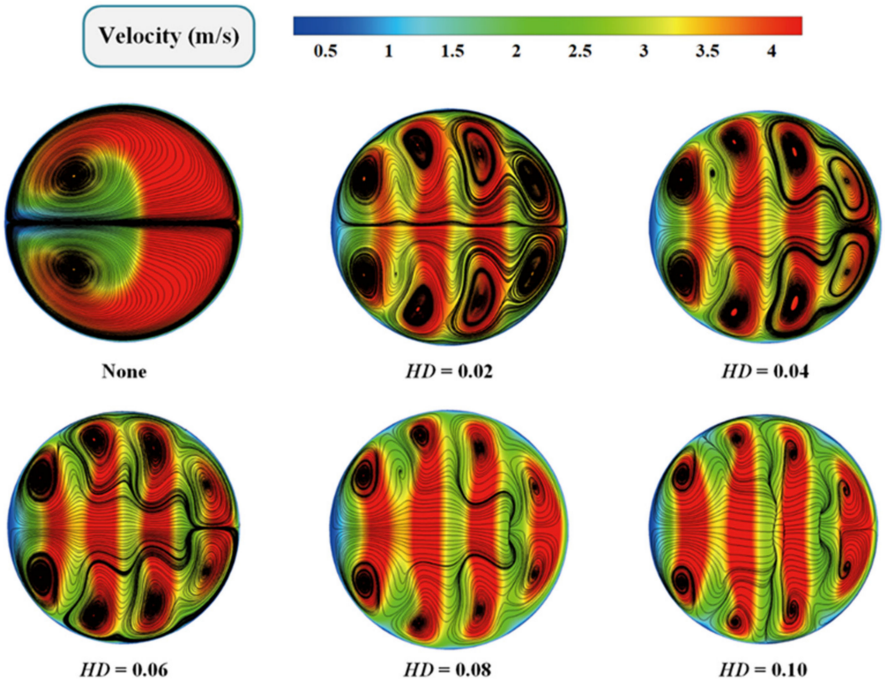

Figure 13. Velocity contour and streamline distribution of 0.67*D* section downstream of 90° bend pipe with different thick-diameter ratio deflectors.

The velocity of the center line (Line D) within 10D downstream of the elbow is further extracted. The downstream velocity of the bend pipe with different thick-diameter ratio flow deflectors is obtained (Figure 14). As can be seen, due to the existence of the flow deflector, the velocity after optimization presents a logarithmic growth trend, while it first decreases and then increases before optimization. This finding shows that the velocity downstream of the bend pipe shows a more stable variation law after optimization. With the increase in HD, the velocity near the elbow outlet gradually decreases and has a slight change when $HD > 0.06$. Influenced by the flow around the deflector, the velocity near the elbow outlet is very small, but it recovers rapidly with the development of the flow and reaches a stable level after 1D. In addition, the stabilized value of velocity after optimization is larger than that before optimization, indicating that the energy loss decreases and the kinetic energy is larger after the installation of the flow deflector. The flow deflector with a certain thickness can reduce the velocity disturbance and make the flow inside the pipe more stable, hence reducing the energy loss of the bend pipe.

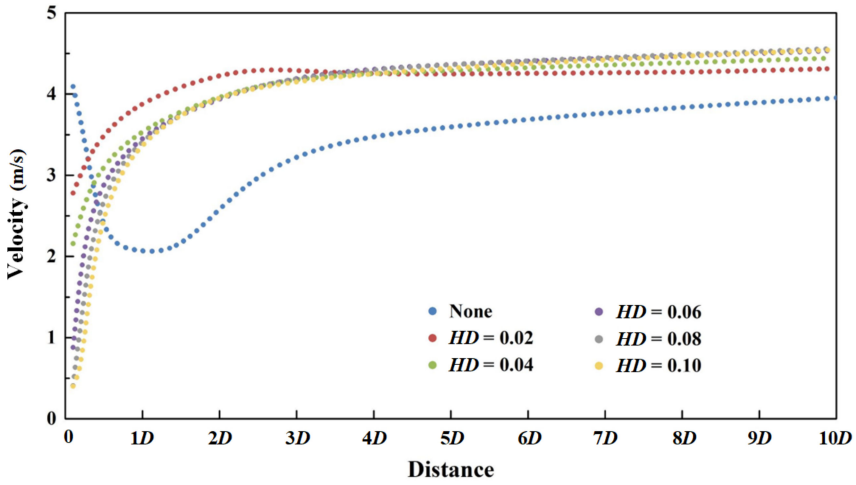

Figure 14. Velocity downstream of 90° bend pipe with different thick-diameter ratio deflectors.

The velocity on horizontal (Line B) and vertical center line (Line C) of the 0.67D cross-section of the elbow is further extracted and dimensionless processing is carried out to obtain the cross-section velocity distribution of the bend pipe with a different thick-diameter ratio flow deflector, as shown in Figure 15. In the horizontal direction, the velocity distribution trend of the downstream cross-section of the bend pipe with flow deflector changes slightly compared with that before optimization. The effect of centrifugal force is dispersed over the enclosed regions, thereby making the velocity on the horizontal axis more uniform and with smaller fluctuations (excluding the near-wall region), which corresponds to the velocity distribution described in Figure 13. Among them, when $HD = 0.06$, the relative change in velocity is small and remains within the range of 0.05. Influenced by the flow around the deflector, the overall velocity on the horizontal axis decreases gradually with the increase in HD.

In the vertical direction, the velocity distribution trend of the downstream cross-section of the bend pipe with flow deflector is improved greatly compared with that before optimization. The elbow region is decomposed into four flow channels by three flow deflectors, so the relative velocity of the downstream cross-section at the elbow outlet shows three troughs and four peaks, which corresponds to the velocity distribution described in Figure 13. Although the phenomenon of velocity fluctuation is still observed, the amplitude of fluctuation is greatly improved compared with before optimization, and the velocity on the vertical center line is relatively more uniform. The flow deflector with a certain thickness can reduce the degree of velocity disturbance and make the flow inside the pipe more uniform, thus enhancing the stability of the bend pipe to a certain extent.

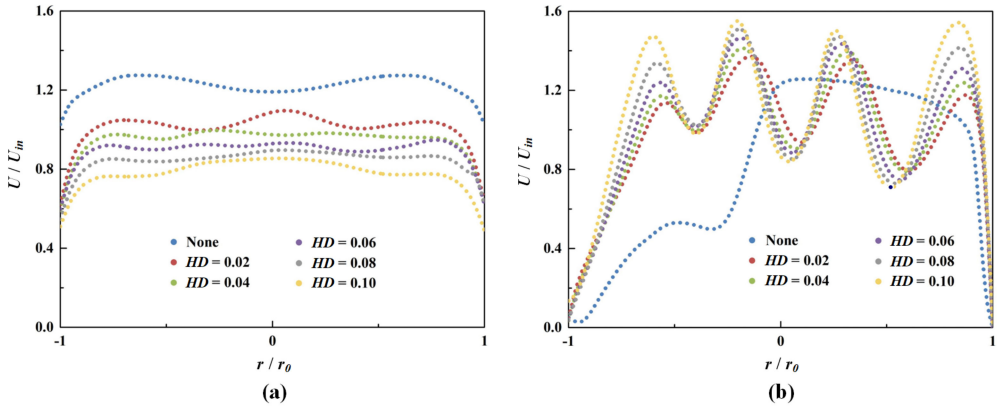

Figure 15. Velocity distribution of (**a**) horizontal and (**b**) vertical centerline of 0.67*D* cross−section downstream of 90° bend pipe with different thick−diameter ratio deflectors installed.

4.2. Different Length-Diameter Ratio

The above analysis indicates that the installation of a certain thickness of the flow deflector can improve the flow characteristics inside the bend pipe, and weaken the influence of the centrifugal force effectively. It can also reduce the energy loss of the bend pipe, thereby increasing the safety and uniformity of the bend pipe to a certain extent. In the process of exploring the influence of the thick-diameter ratio of the flow deflector on the flow characteristics, the optimal effect is best when the deflector with $HD = 0.06$ is installed.

To further study the influence of the length-diameter ratio on the flow characteristics, it is kept at 0.06 in this paper, and the velocity on horizontal (Line B) and vertical center lines (Line C) of 0.67*D* cross-section downstream of the elbow are extracted. Dimensionless processing is carried out for the extracted data, and the cross-section velocity distribution of the bend pipe with different length-diameter ratio deflectors is obtained (Figure 16). In the horizontal and vertical directions, the global velocity distribution of a downstream cross-section of bend pipe with a different length-diameter ratio does not change significantly. However, locally, the relative velocity in both directions decreases first and then increases, with the maximum fluctuation amplitude when $LR = 0.13$ and the minimum value when $LR = 0.30$. Therefore, the increase in the sharp-end length of the flow deflector can improve the velocity uniformity to a certain extent, but has minimal influence on the flow characteristics of the bend pipe.

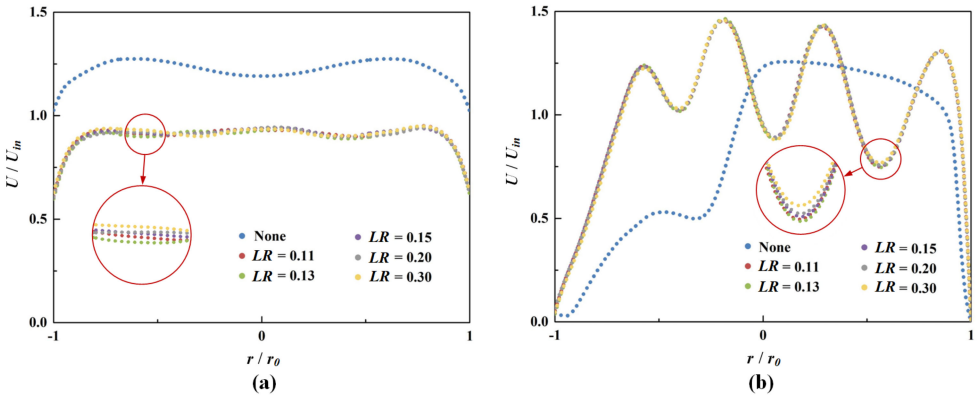

Figure 16. Velocity distribution of (**a**) horizontal and (**b**) vertical center line at 0.67*D* cross−section downstream of 90° bend pipe with different length−diameter ratio deflectors installed.

5. Conclusions and Prospects

In this paper, 3D circular bend pipe models with different bending angles are established. The flow inside the bend pipe is simulated by Fluent© commercial software. The

numerical results are in good agreement with the existing literature. The influence of bending angle on flow field distribution is analyzed. The larger the bending angle is, the more obvious the flow distribution and even the unevenness at the elbow will be, thereby resulting in poor stability. Furthermore, the difference in bending angle can affect the wake flow downstream of the elbow. With the increment in bending angle, the distance required to restore the flow uniformity also increases. The pressure energy loss of the bend pipe with different bending angle is investigated. The results show that with the increase in bending angle, the global pressure loss presents a trend of "increase-decrease-increase". The closer the bending angle is to 90°, the greater the influence of centrifugal force is on the flow, and the more obvious the secondary flow phenomenon will be.

In view of the non-uniformity and instability of the flow inside the bend pipe, the 90° bend pipe with the greatest influence is selected to optimize the local structure. Three flow deflectors are installed at equal intervals in the elbow. The improvement of flow characteristics of the bend pipe with different thickness-diameter ratio and length-diameter ratio is compared. The flow deflector with a certain thickness can weaken the local accumulation of pressure energy at the elbow effectively and adjust the structure of secondary flow, thereby shortening the distance for the wake flow to recover smoothly downstream of the elbow. With the increase in HD of the flow deflector, the optimized effect becomes better at first and then becomes worse, and reaches the best effect at 0.06. In addition, the increase in LR can improve the velocity uniformity to a certain extent, but has minimal influence on the flow characteristics of the bend pipe compared with HD. This study aims to investigate and improve the flow characteristics of a multi-structure bend pipe to make it suitable for more complex working conditions and to provide a certain theoretical basis.

In future research, the bending angle in a smaller local range can be also explored, especially the specific change law of flow characteristics in the bend pipe at a small bending angle. At the same time, the structure of the flow deflector can be improved more extensively to select the structure with better performance improvement.

Author Contributions: Methodology and validation, J.Z., D.W., W.W. and Z.Z.; formal analysis, D.W. and W.W.; writing—review and editing, D.W. and W.W. All authors have read and agreed to the published version of the manuscript.

Funding: This research was funded by Key Research and Development Program of Zhejiang Province (Grant No. 2022C03140).

Institutional Review Board Statement: Not applicable.

Informed Consent Statement: Not applicable.

Data Availability Statement: Not applicable.

Conflicts of Interest: The authors declare no conflict of interest.

References

1. Wu, Y.; Liu, S.; Dou, H.-S.; Wu, S.; Chen, T. Numerical prediction and similarity study of pressure fluctuation in a prototype Kaplan turbine and the model turbine. *Comput. Fluids* **2012**, *56*, 128–142. [CrossRef]
2. Kamyar, A.; Aminossadati, S.M.; Leonardi, C.R.; Sasmito, A.P.; Poncet, S. Flow characterisation of monopropylene glycol ice slurry through a horizontal U-bend: A numerical approach. *Eur. J. Mech. B/Fluids* **2020**, *82*, 93–105. [CrossRef]
3. Fellouah, H.; Castelain, C.; Ould-El-Moctar, A.; Peerhossaini, H. The Dean instability in power-law and Bingham fluids in a curved rectangular duct. *J. Non-Newton. Fluid Mech.* **2010**, *165*, 163–173. [CrossRef]
4. Skillen, A.; Zimon, M.J.; Sawko, R.; Tunstall, R.; Moulinec, C.; Emerson, D.R. Thermal transients in a U-bend. *Int. J. Heat Mass Transf.* **2020**, *148*, 119039. [CrossRef]
5. Kumar, P.; Singh, J. Computational study on effect of Mahua natural surfactant on the flow properties of heavy crude oil in a 90° bend. *Mater. Today Proc.* **2021**, *43*, 682–688. [CrossRef]
6. Akar, S.; Esfahani, J.A.; Shaegh, S.A.M. A numerical investigation on the Magnetophoretic-guided stem cells delivery in a bend blood vessel. *J. Magn. Magn. Mater.* **2019**, *498*, 166110. [CrossRef]
7. Dean, W.R. Fluid motion in a curved channel. *Proc. R. Soc. A Math. Phys. Eng. Sci.* **1928**, *121*, 402–420.
8. Hashemi, A.; Fischer, P.F.; Loth, F. Direct numerical simulation of transitional flow in a finite length curved pipe. *J. Turbul.* **2018**, *19*, 664–682. [CrossRef]

9. Canton, J.; Schlatter, P.; Örlü, R. Modal instability of the flow in a toroidal pipe. *J. Fluid Mech.* **2016**, *792*, 894–909. [CrossRef]
10. Ji, Y.; Wilson, C.; Chen, H.-H.; Ma, H. Particle shape effect on heat transfer performance in an oscillating heat pipe. *Nanoscale Res. Lett.* **2011**, *6*, 296. [CrossRef] [PubMed]
11. Kalpakli, A.; Örlü, R. Turbulent pipe flow downstream a 90° pipe bend with and without superimposed swirl. *Int. J. Heat Fluid Flow* **2013**, *41*, 103–111. [CrossRef]
12. Kalpakli, A.; Örlü, R.; Alfredsson, P. Vortical patterns in turbulent flow downstream a 90° curved pipe at high Womersley numbers. *Int. J. Heat Fluid Flow* **2013**, *44*, 692–699. [CrossRef]
13. Lupi, V.; Canton, J.; Schlatter, P. Global stability analysis of a 90°-bend pipe flow. *Int. J. Heat Fluid Flow* **2020**, *86*, 108742. [CrossRef]
14. Wang, Z.; Örlü, R.; Schlatter, P.; Chung, Y.M. Direct numerical simulation of a turbulent 90° bend pipe flow. *Int. J. Heat Fluid Flow* **2018**, *73*, 199–208. [CrossRef]
15. Wang, T.; Tu, S.; Dong, D.; Guo, L.; Joseph, D.D.; Matsumoto, Y.; Sommerfeld, Y.; Wang, Y. Numerical simulation of flow characteristic in three-dimensional bend pipes. In Proceedings of the 6th International Symposium on Multiphase Flow, Heat Mass Transfer and Energy Conversion, Xi'an, China, 11–15 July 2009; pp. 424–428.
16. Dutta, P.; Saha, S.K.; Nandi, N.; Pal, N. Numerical study on flow separation in 90° pipe bend under high Reynolds number by k-ε modelling. *Eng. Sci. Technol. Int. J.* **2016**, *19*, 904–910. [CrossRef]
17. Ran, L.Y.; Zhao, J.; Qin, H.B.; Hu, S.G.; Tian, X.L. The Analysis of Field Characteristics and Measurement for Centrifugal Fan and 90° Bend Pipe. *Appl. Mech. Mater.* **2014**, *628*, 266–269. [CrossRef]
18. Zhang, H.; Zhang, X.; Sun, H.; Chen, M.; Lu, X.; Wang, Y.; Liu, X. Pressure of Newtonian fluid flow through curved pipes and elbows. *J. Therm. Sci.* **2013**, *22*, 372–376. [CrossRef]
19. Chowdhury, R.R.; Biswas, S.; Alam, M.; Islam, A.K.M.S. Turbulent flow analysis on bend and downstream of the bend for different curvature ratio. In Proceedings of the 11th International Conference on Mechanical Engineering, Dhaka, Bangladesh, 18–20 December 2015; p. 040020.
20. Kim, Y.-J.; Oh, C.-S. Limit loads for pipe bends under combined pressure and in-plane bending based on finite element limit analysis. *Int. J. Press. Vessel. Pip.* **2006**, *83*, 148–153. [CrossRef]
21. Li, J.; Zhou, C.-Y.; Xue, J.-L.; He, X.-H. Limit loads for pipe bends under combined pressure and out-of-plane bending moment based on finite element analysis. *Int. J. Mech. Sci.* **2014**, *88*, 100–109. [CrossRef]
22. Qian, X.; Yang, Y.; Lee, S.W. Design and evaluation of the lab-ccale shell and tube heat exchanger (STHE) for poultry litter to energy production. *Processes* **2020**, *8*, 500. [CrossRef]
23. Zhang, Q.; Wu, F.; Yang, Z.; Li, G.; Zuo, J. Simulation of the Transient Characteristics of Water Pipeline Leakage with Different Bending Angles. *Water* **2019**, *11*, 1871. [CrossRef]
24. Li, S.-J.; Zhou, C.-Y.; Li, J.; Pan, X.-M.; He, X.-H. Effect of bend angle on plastic limit loads of pipe bends under different load conditions. *Int. J. Mech. Sci.* **2017**, *131–132*, 572–585. [CrossRef]
25. Silambarasan, R.; Veerappan, A.R.; Shanmugam, S. Effect of structural deformations and bend angle on the collapse load of pipe bends subjected to in-plane closing bending moment. *World J. Eng.* **2021**, *19*, 594–603. [CrossRef]
26. Kim, Y.-J.; Lee, K.-H.; Oh, C.-S.; Yoo, B.; Park, C.-Y. Effect of bend angle on plastic loads of pipe bends under internal pressure and in-plane bending. *Int. J. Mech. Sci.* **2007**, *49*, 1413–1424. [CrossRef]
27. Li, S.; Zhou, C.; Li, J.; Miao, X. Effect of Bend Angle on Plastic Limit Loads of Pipe Bends Under In-Plane Bending Moment. In Proceedings of the ASME Pressure Vessels and Piping Conference, Vancouver, BC, Canada, 17–21 July 2016.
28. Bezyan, B.; Porkhial, S.; Mehrizi, A.A. 3-D simulation of heat transfer rate in geothermal pile-foundation heat exchangers with spiral pipe configuration. *Appl. Therm. Eng.* **2015**, *87*, 655–668. [CrossRef]
29. Arun, G.; Babu, S.K.; Natarajan, S.; Kulasekharan, N. Study of flow behaviour in sharp and mitred pipe bends. *Mater. Today Proc.* **2019**, *27*, 2101–2108. [CrossRef]
30. Valsala, R.R.; Son, S.W.; Suryan, A.; Kim, H.D. Study on reduction in pressure losses in pipe bends using guide vanes. *J. Vis.* **2019**, *22*, 795–807. [CrossRef]
31. Enayet, M.; Gibson, M.; Taylor, A.; Yianneskis, M. Laser-Doppler measurements of laminar and turbulent flow in a pipe bend. *Int. J. Heat Fluid Flow* **1982**, *3*, 213–219. [CrossRef]
32. Sudo, K.; Sumida, M.; Hibara, H. Experimental investigation on turbulent flow in a circular-sectioned 90-degree bend. *Exp. Fluids* **1998**, *25*, 42–49. [CrossRef]
33. Sudo, K.; Sumida, M.; Hibara, H. Experimental investigation on turbulent flow through a circular-sectioned 180° bend. *Exp. Fluids* **2000**, *28*, 51–57. [CrossRef]
34. Carlsson, C.; Alenius, E.; Fuchs, L. Swirl switching in turbulent flow through 90° pipe bends. *Phys. Fluids* **2015**, *27*, 085112. [CrossRef]
35. Lin, Z.; Wang, D.; Tao, J.; Zhu, Z.; Guo, X. Transient Regulating Characteristics of V-Port Ball Valve in Opening and Closing Process. *J. Fluids Eng.* **2022**, *144*, 101201. [CrossRef]
36. Wang, X.; He, M. Numerical simulation of wing-body junction turbulence flow. *Appl. Math. Mech.* **1993**, *14*, 581–587.
37. Batchelor, G.K. *An Introduction to Fluid Dynamics*; Cambridge University Press: Cambridge, UK, 1967.
38. Shih, T.-H.; Liou, W.W.; Shabbir, A.; Yang, Z.; Zhu, J. A new k-ϵ eddy viscosity model for high reynolds number turbulent flows. *Comput. Fluids* **1995**, *24*, 227–238. [CrossRef]

39. Akin, A.; Kahveci, H.S. Effect of turbulence modeling for the prediction of flow and heat transfer in rotorcraft avionics bay. *Aerosp. Sci. Technol.* **2019**, *95*, 105453. [CrossRef]
40. Tian, Z.F.; Tu, J.Y.; Yeoh, G. CFD Studies of Indoor Airflow and Contaminant Particle Transportation. *Part. Sci. Technol.* **2007**, *25*, 555–570. [CrossRef]
41. Qian, Z.D.; Hu, X.Q.; Huai, W.X.; Amador, A. Numerical simulation and analysis of water flow over stepped spillways. *Sci. China Ser. E Technol. Sci.* **2009**, *52*, 1958–1965. [CrossRef]
42. Moukalled, F.; Mangani, L.; Darwish, M. *The Finite Volume Method in Computational Fluid Dynamics*; Springer International Publishing: Berlin/Heidelberg, Germany, 2016.
43. Liu, L.; Li, S.; Guo, P.; Wang, X. Natural wind impact analysis of transiting test method to measure wind pressure coefficients. *Wind. Struct.* **2020**, *30*, 199–210. [CrossRef]
44. Xu, B.; Feng, J.; Shen, X.; Zhang, D.; Zhang, W. Numerical investigation of cavitation suppression in an inducer for water and liquid nitrogen with emphasis on thermodynamic effect. *J. Braz. Soc. Mech. Sci. Eng.* **2021**, *43*, 212. [CrossRef]
45. Zou, Q.; Li, Z.; Wu, H.; Kuang, R.; Hui, Y. Wind pressure distribution on trough concentrator and fluctuating wind pressure characteristics. *Sol. Energy* **2015**, *120*, 464–478. [CrossRef]
46. Cui, B.; Lin, Z.; Zhu, Z.; Wang, H.; Ma, G. Influence of opening and closing process of ball valve on external performance and internal flow characteristics. *Exp. Therm. Fluid Sci.* **2017**, *80*, 193–202. [CrossRef]
47. Tao, J.; Lin, Z.; Ma, C.; Ye, J.; Zhu, Z.; Li, Y.; Mao, W. An Experimental and Numerical Study of Regulating Performance and Flow Loss in a V-Port Ball Valve. *ASME J. Fluids Eng.* **2020**, *142*, 021207. [CrossRef]